Mon. Not. R. astr. Soc. (1989) **241**, 575–593

High-resolution observations of interstellar CH and CH^+ towards the Scorpius OB1 association

Ian A. Crawford★ *University of London Observatory (Department of Physics and Astronomy, University College London), Mill Hill Park, London NW7 2QS*

Accepted 1989 May 10. Received 1989 May 5; in original form 1989 January 23

Summary. High-resolution observations ($\lambda/\Delta\lambda = 10^5$) of interstellar CH and CH^+ towards nine stars in the Sco OB1 association are presented. Several velocity components were observed towards most stars and these are interpreted to arise in foreground diffuse molecular clouds. Three distinct types of absorption component were found: components present in both CH and CH^+, components present in CH^+ only, and components present in CH only. Possible origins for these three classes of component are discussed. Although shock models are generally thought to be necessary for the production of CH^+ in interstellar clouds, it was found that, for those components observed in both species, the very small velocity differences observed between them ($\lesssim 0.9$ km s^{-1}) correspond to shock velocities that are too small for significant CH^+ production. However, on the basis of published shock models, it is suggested that the components observed in CH^+ alone may arise in shocked low-density clouds with only a small fractional abundance of molecular hydrogen.

1 Introduction

The Scorpius OB1 association ($l = 343°$, $b = +1°$) is situated in the Sagittarius spiral arm at a distance of about 1900 pc from the Sun (Humphreys 1978). It is spread over an area of approximately 1° by 2° and contains the bright and compact open cluster NGC 6231. A sketch showing the relative positions of the stars observed here has been given by Crawford, Barlow & Blades (1989; their fig. 1); photographs of the region can be found in Bok, Bok & Graham (1966) and on ESO Sky Survey prints B332 and R332.

The interstellar extinction towards the Sco OB1 association has been studied by van Genderen, Bijeveld & van Groningen (1984). The extinction is not uniform across the association: for the stars of interest here, van Genderen *et al.* found the colour excesses to be in the range 0.35–0.79 mag (*cf.* Table 1). From their photometry of about 60 foreground stars, van Genderen *et al.* found that most of this extinction occurs within about 700 pc of the Sun, and thus within the local (Orion) spiral arm. Schild, Neugebauer & Westphal (1971) came to similar conclusions. Note that spiral density wave theories predict, and observations (e.g.

★ Present address: Mt Stromlo and Siding Spring Observatories, Private Bag, Woden P.O., Canberra, ACT 2606, Australia.

Vogel, Kulkarni & Scoville 1988) confirm, that the densest interstellar regions in spiral galaxies lie on the inner edges of the spiral arms, with the OB associations being found several hundred parsecs further out. Such a picture is consistent with the extinction observed towards Sco OB1 occurring within several hundred parsecs of the Sun and the remainder of the line-of-sight being relatively clear (*cf.* fig. 1 of Lynds 1980).

This paper discusses observations of the molecules CH and CH^+ that were obtained as part of a detailed study of the interstellar medium towards the Sco OB1 association. High-resolution observations of the interstellar atomic species Na I and Ca II resulting from this study have been presented by Crawford *et al.* (1989), and a study of the interstellar ultraviolet lines observed towards six members of the association has been reported by Crawford (1989).

2 Observations

High-resolution observations of interstellar CH and CH^+ towards nine stars in the Sco OB1 association were obtained with the Mt Stromlo 74-inch telescope and coudé échelle spectrograph during 1986 June and 1987 June. Table 1 lists the stars observed, their V magnitudes (from Hoffleit & Jaschek 1982), colour excesses (van Genderen *et al.* 1984), and the exposure times for each spectral region. All the CH^+ observations were obtained in 1987, while CH was observed in both years.

The spectrograph was used with the 130-inch focal length camera, and the observations (with the exception of the CH^+ observation towards HD 152236) were performed with a 250-μm slit width, corresponding to a velocity resolution of 3 km s^{-1} (FWHM). The CH^+ observation of HD 152236 was performed with a 125-μm slit, or 1.5 km s^{-1} resolution. The resolution of this instrument has been discussed in more detail by Crawford, Rees & Diego (1987). The detector was a Photon Counting Array (PCA, Stapinski, Rodgers & Ellis 1981) which has a spectral coverage of about 4 Å at these wavelengths. Table 2 gives the rest

Table 1. The V magnitudes, colour excesses and exposure times for the stars observed.

Star HD	V	$E(B-V)$	CH No. of exps.	CH Total exp. time (s)	CH^+ No. of exps.	CH^+ Total exp. time (s)
151804	5.3	0.35	1	3600	1	3204
152234	5.5	0.46	2	6000	1	3209
152235	6.4	0.79	4	7726	1	8415
152236	4.8	0.69	1	3000	1	5459
152248	6.1	0.44	2	6000	1	4600
152249	6.5	0.48	2	6000	3	8594
152270	6.7	0.48	2	6000	1	7200
152408	5.8	0.47	1	3600	1	6004
152424	6.4	0.69	4	9131	1	7200

Table 2. Rest wavelengths and instrumental characteristics for the observed interstellar molecular lines. $\Delta\lambda_{PCA}$ is the spectral coverage of the detector.

Mol.	Trans.	Line	λ_0 (Å)	Ref.	Disp. (Å mm^{-1})	$\Delta\lambda_{PCA}$ (Å)
CH	$A^2\Delta - X^2\Pi$	$R_2(1)$	4300.313	1	0.356	4.00
CH^+	$A^1\Pi - X^1\Sigma^+$	R(0)	4232.548	2	0.376	4.23

References: (1) quoted by Black & van Dishoeck (1988) based on the work of Bernath (1987) and Brazier & Brown (1984); (2) given by Lambert & Danks (1986) based on the wavenumbers of Carrington & Ramsey (1982).

wavelengths of the lines observed, the dispersion and the spectral range covered by the PCA detector in each case.

For each spectrum the two-dimensional PCA image was divided by a flat-field and the spectrum was extracted using the FIGARO program (described by Fuller 1988) on the UCL STARLINK node. The background (obtained from rows adjacent to the spectrum) was subtracted, and the spectrum was wavelength calibrated by means of a Th–Ar lamp. Rest wavelengths for the Th and Ar lines were taken from Giacchetti, Stanley & Zalubas (1970) and Norlén (1973) respectively. For both spectral regions three lines from the lamp were found to lie on the detector, and linear fits to the positions of these lines yielded residuals of $\lesssim 2$ mÅ. The CH line was found to be bracketed by the comparison lines, while for CH^+ extrapolation (by about 1.7 Å) was necessary [note that although this extrapolation will have overestimated the wavelength of the CH^+ line, measurements made in a neighbouring spectral region (within 6 Å of the CH^+ wavelength) where the Th–Ar lines are more closely spaced, indicated that this overestimate amounts to $\lesssim 1$ mÅ, or only 0.07 km s^{-1}]. Once calibrated in wavelength, all spectra were converted to the heliocentric velocity frame and all multiple exposures (Table 1) were averaged.

Table 3. Equivalent widths (w_λ), heliocentric radial velocities (v), velocity dispersions (b) and column densities (N) for the interstellar CH lines observed towards stars in the Sco OB1 association. The equivalent widths are summed over all velocity components. Δb and ΔN are the ranges of b and N that give acceptable fits to the observed profiles.

Star HD	w_λ mÅ	v km s^{-1}	b km s^{-1}	Δb km s^{-1}	N $\times 10^{12}$ cm^{-2}	ΔN $\times 10^{12}$ cm^{-2}
151804	$\lesssim$2.0	...	...	...	$\lesssim$2.4	...
152234	5.9±0.9	+2.2	3.0	2.0–3.5	9.0	7.0–10
152235	33±3	−5.0	2.5	1.5–3.0	33	24–37
		+0.2	1.5	1.0–2.0	13	11–15
152236	20±3	−9.9	1.8	1.5–2.5	7.4	7.0–8.0
		−3.3	2.5	1.5–4.0	5.5	4.0–8.0
		+0.8	1.3	1.0–1.6	12	10–13
152248	8.2±1.2	+2.2	2.5	2.0–3.0	10	9–12
152249	3.7±1.2	+2.2	1.5	1.0–2.5	4.5	3.5–6.0
152270	8.2±1.3	+2.2	1.2	1.0–1.6	12	10–14
152408	$\lesssim$9.0	...	...	...	$\lesssim$11	...
152424	33±4	−17.0	2.0	1.0–4.0	4.0	2.0–9.0
		−11.5	3.0	2.0–3.5	20	13–23
		−4.1	1.4	1.0–2.0	6.0	5.0–7.0
		+1.0	1.5	1.0–2.0	6.5	5.5–7.5

Table 4. Equivalent widths, radial velocities, velocity dispersions and column densities for the interstellar CH^+ lines observed towards Sco OB1. See caption to Table 3 for details.

Star HD	w_λ mÅ	v km s^{-1}	b km s^{-1}	Δb km s^{-1}	N $\times 10^{12}$ cm^{-2}	ΔN $\times 10^{12}$ cm^{-2}
151804	7.3±1.9	−5.2	2.2	1.5–3.0	8.0	6.0–10
152234	20±3	−3.9	5.0	3.0–7.00	9.0	5.0–11
		+3.1	2.5	2.0–3.0	19	15–22
152235	42±5	−4.7	2.5	2.0–3.0	48	40–55
		+1.1	2.5	2.0–4.0	10	8.0–15
152236	6.1±2.9	−7.7	1.5	1.0–2.0	6.0	4.0–8.0
152248	11±3	+3.1	3.5	3.0–4.5	12	8.0–15
152249	15±3	−3.4	2.5	2.0–4.0	8.0	6.0–11
		+3.1	2.0	1.5–3.0	11	9.0–14
152270	13±3	+3.1	2.0	1.5–2.5	14	11–17
152408	12±4	−3.3	2.0	1.5–3.0	7.0	5.0–10
152424	27±5	−11.4	2.0	1.5–2.5	21	18–25
		−3.9	2.0	1.0–3.0	10	7.0–13
		+4.1	2.0	1.5–3.0	7.0	5.0–9.0

3 Line profile analysis and column densities

In order to determine the molecular column densities and velocity dispersions, theoretical line profiles were calculated using the BACH program, due originally to Davenhall (1977). The theory of interstellar line profiles, on which this program is based, was described by Strömgren (1948), and has been reviewed recently by Cowie & Songaila (1986). Each absorption component is described by a radial velocity, v, column density, N, and velocity dispersion parameter, b. The parameters v, b and N were adjusted by trial and error until a satisfactory fit to each spectrum was obtained. The range of b and N values that produced equally satisfactory fits was also determined in each case. The adopted oscillator strengths were: 5.09×10^{-3} for the CH line (Danks, Federman & Lambert 1984), and 5.50×10^{-3} for CH^+ (Lambert & Danks 1986).

The $R_2(1)$ line of CH is split because of Λ-doubling in the ground state of the molecule. The splitting amounts to 20.8 mÅ, or 1.45 km s^{-1} (Baird & Bredohl 1971) and, although not resolved in the present study, it was found to broaden the profiles. This was allowed for by performing the line profile calculation separately for each component, and combining them by adding the optical depths due to each. There is no Λ-doubling in the ground state of CH^+.

Tables 3 and 4 give the line profile parameters, together with the measured equivalent widths, for the CH and CH^+ observations, respectively. These tables show that the velocity

dispersions were found to be small, with b values generally between 1 and 3 km s^{-1}. No significant difference was found between the b values of CH and CH$^+$. Diffuse interstellar clouds are generally assumed to have a temperature of about 80 K (based on observations of the rotational excitation of molecular hydrogen, e.g. Savage *et al.* 1977), so these b values imply turbulent velocities of ~ 0.7–2 km s^{-1} (*cf.* equation 3.7 of Cowie & Songaila 1986). Thus, if these components are truly single, the clouds are either significantly hotter than expected for diffuse clouds or are subject to supersonic turbulence.

The spectra are shown in Figs 1–9. The observed spectra have been smoothed by averaging adjacent pixels and are plotted as histograms. [Note that averaging adjacent pixels has not degraded the resolution since the instrumental response of this instrument (obtained by convolving the grating interference pattern with the projected slit width, Crawford *et al.* 1987) has a FWHM of about 7 pixels for these observations.] The smooth lines in these figures are the theoretical profiles calculated with the parameters given in Tables 3 and 4. These profiles have been convolved with the instrumental response function of the spectrograph so that they can be directly compared with the observations. Note that the measuring error on the velocities, i.e. the accuracy with which the profiles generated by BACH can be matched to the data, is about ± 0.4 km s^{-1}.

4 Comparison with previous results

Danks, Federman & Lambert (1984), with a better signal-to-noise ratio than obtained here, found column densities of $\sim 5 \times 10^{12}$ cm^{-2} and 5.3×10^{12} cm^{-2} for CH towards HD 151804 and 152408, respectively. The latter is consistent with the upper limit given in Table 3, although the former exceeds the upper limit obtained here by a factor of two. Danks *et al.* identified two velocity components in CH towards HD 151804, separated by about 3 km s^{-1}. There is no hint of this structure in Fig. 1(b), presumably because of an insufficient signal-to-noise ratio.

Lambert & Danks (1986) give CH$^+$ column densities of 8.3×10^{12} cm^{-2} for HD 151804, in good agreement with that given in Table 4, and 12.0×10^{12} cm^{-2} for the main component towards HD 152236, approximately twice the value found here. The radial velocities obtained for these lines by Lambert & Danks are in good agreement with those found here, although in both cases their values are about 0.6 km s^{-1} more positive than those given in Table 4. Finally, Lambert & Danks found a weaker component, with a velocity about 9 km s^{-1} more positive than the main component, towards HD 152236. There is a slight dip in the spectrum presented in Fig. 4(a) which might correspond to this component, although the signal-to-noise ratio is not sufficient to make a definite identification.

5 Comparison of CH and CH$^+$ velocities

Reference to Figs 1–9, and Tables 3 and 4, shows that most of the stars have CH$^+$ and CH components with heliocentric velocities that are very similar, with velocity differences between them in the range 0.1–0.9 km s^{-1}. Note that this difference always has the same sense: the CH$^+$ velocities are always larger (more positive) than the CH velocities. Table 5 identifies those CH and CH$^+$ components which, from an inspection of Figs 1–9, are thought to corresond. The magnitude of the velocity differences between them is given in each case, as is the $N(\mathrm{CH}^+)/N(\mathrm{CH})$ ratio on the assumption that both molecules are physically associated in these components.

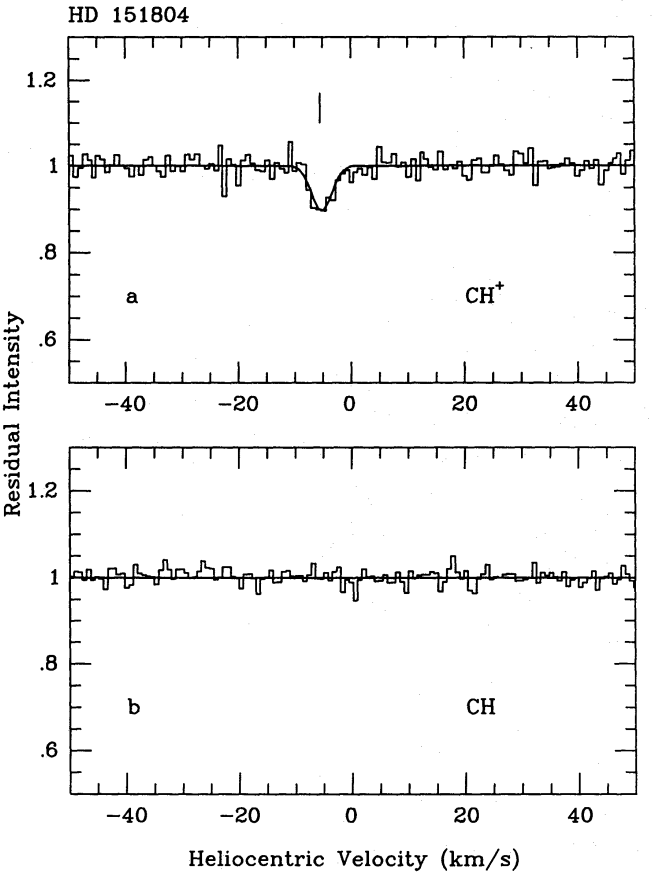

Figure 1

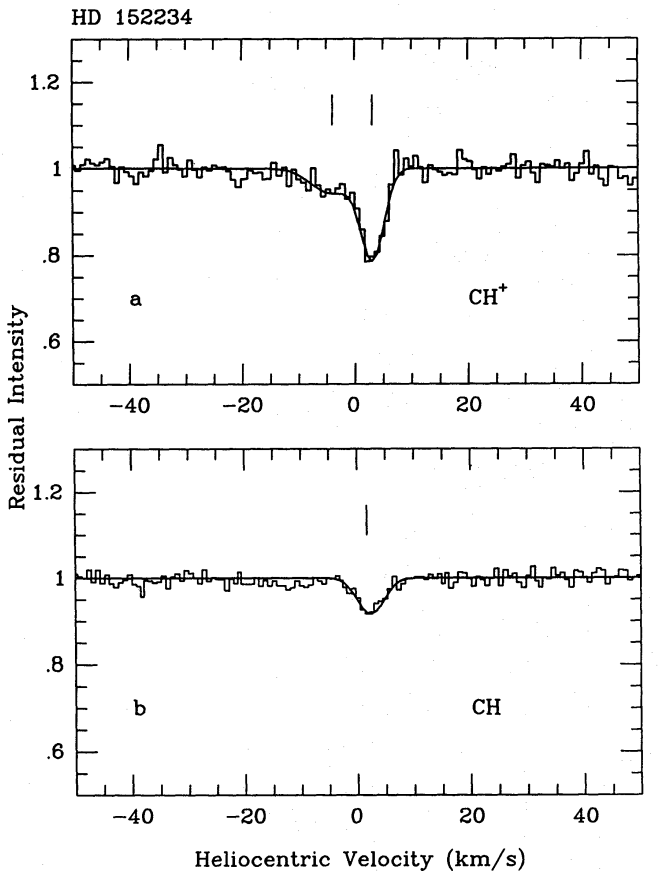

Figure 2

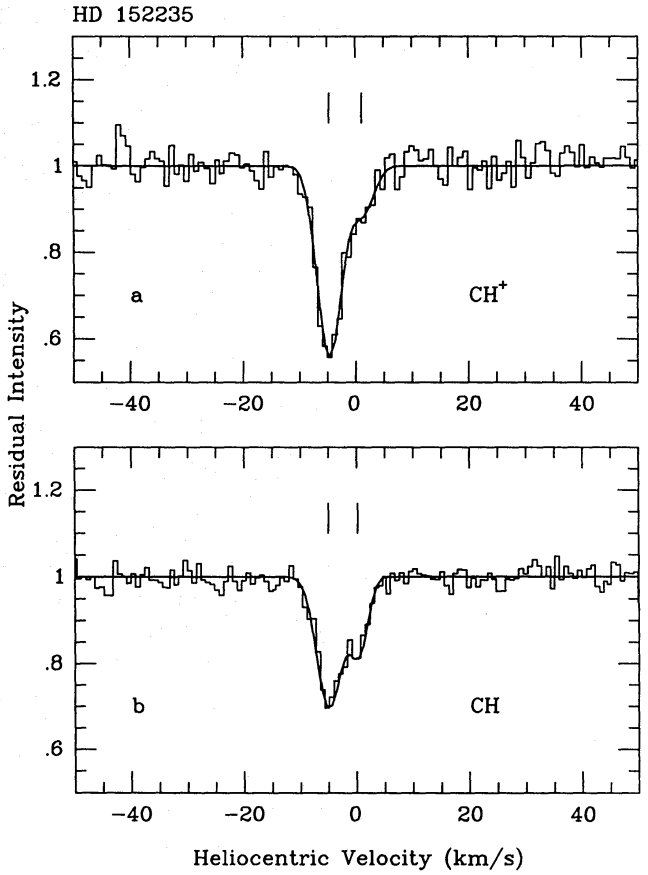

Figure 3

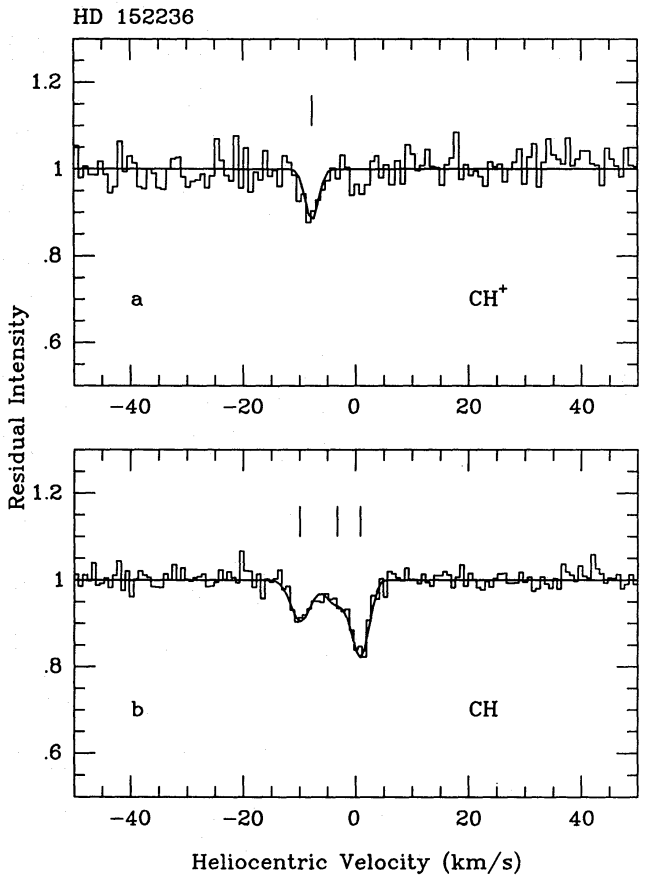

Figure 4

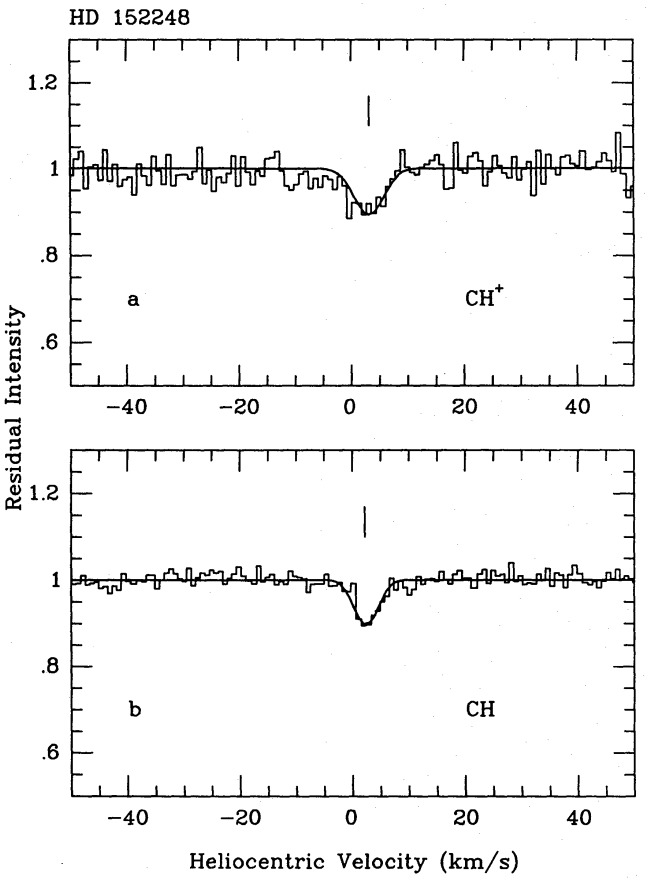

Figure 5

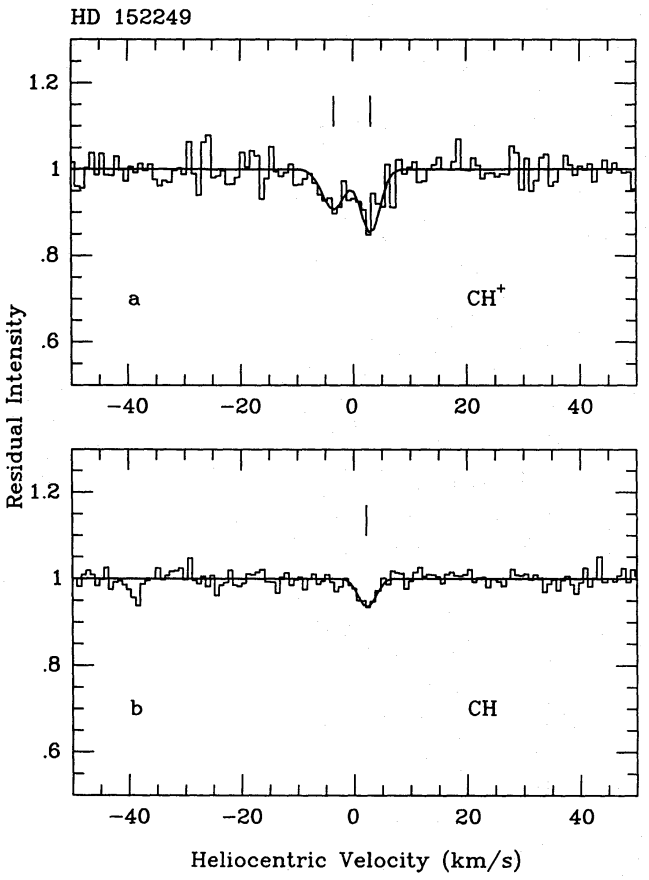

Figure 6

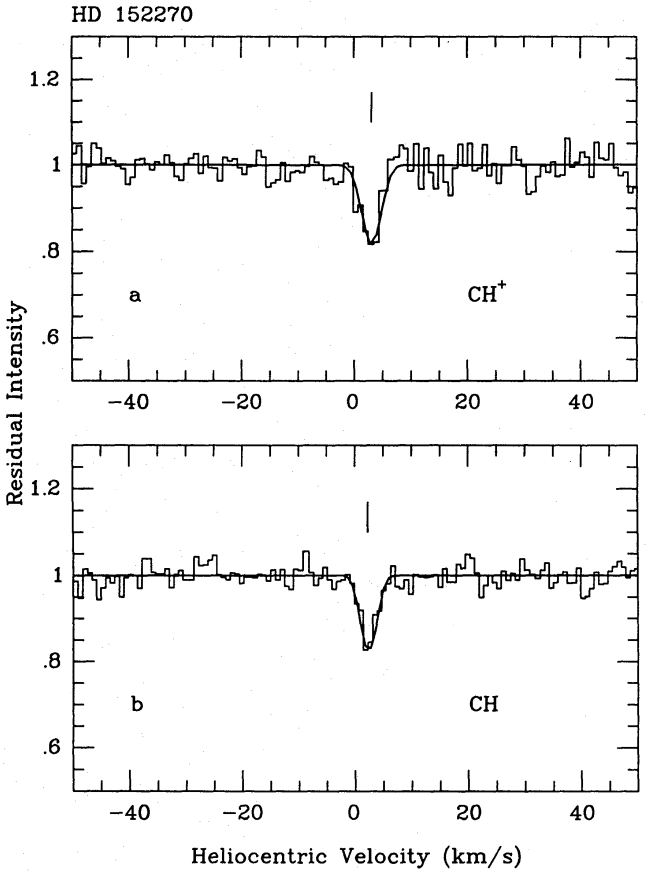

Figure 7

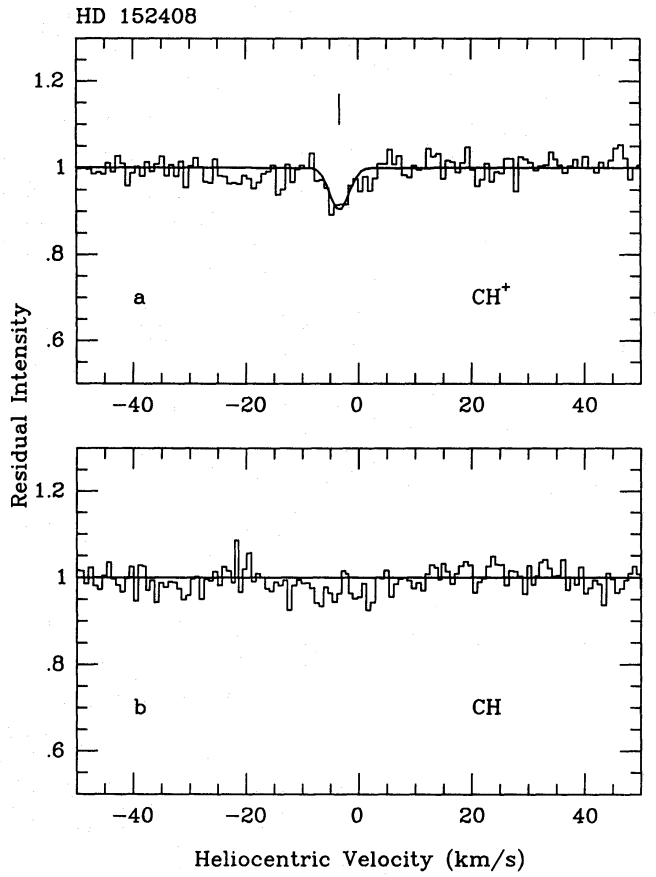

Figure 8

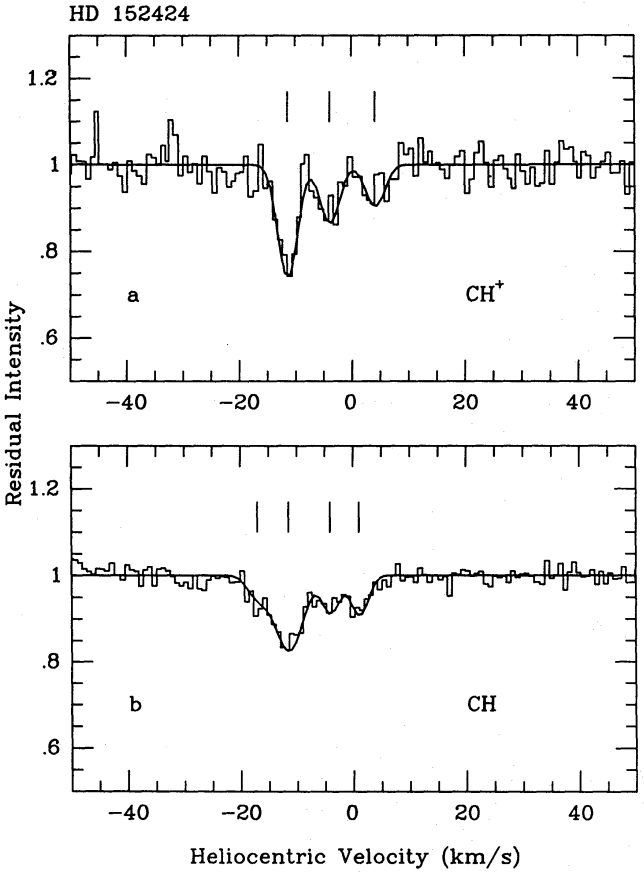

Figure 9

Figures 1–9. Observations of (a) CH^+ and (b) CH towards nine members of the Sco OB1 association. In each case, the observed spectrum is represented as a histogram (where each bin is the mean of two recorded data points) and the solid line is a model profile with the parameters given in Tables 3 and 4. Vertical tick marks indicate the positions of identified velocity components.

Since the measuring error for each velocity component is about ± 0.4 km s^{-1}, it is clear that only for the larger of these apparent velocity shifts is there any likelihood of them being physically significant. Moreover, since the residuals obtained during the wavelength calibration ($\lesssim 2$ mÅ, Section 2) correspond to additional velocity errors of up to 0.14 km s^{-1}, and since some uncertainties must exist on the adopted rest wavelengths [for example, Carrington & Ramsey (1982) state an absolute uncertainty of up to 0.02 cm^{-1} on their wavenumbers, corresponding to a velocity error of 0.25 km s^{-1}] even an apparent difference of 0.9 km s^{-1} may not be real.

It is worth noting that much previous work has made use of the CH rest wavelength of 4300.321 Å given by Moore & Broida (1959). This differs by 0.54 km s^{-1} from the value recommended by Black & van Dishoeck (1988), based on the work of Bernath (1987) and Brazier & Brown (1984). Use of the earlier value would lead to a larger velocity difference between CH and CH^+.

6 The velocity structure

All the molecular absorption occurs at low heliocentric velocities, with $-10 \lesssim v_{\rm helio} \lesssim +5$ km s^{-1} for all stars except HD 152424. Even for this star, however, no molecular absorption

Table 5. Corresponding CH^+ and CH velocity components and their CH^+/CH ratios [$\Delta v \equiv v(CH^+) - v(CH)$].

Star HD	$v(CH^+)$ km s^{-1}	v(CH) km s^{-1}	Δv km s^{-1}	$N(CH^+)/N(CH)$
151804	−5.2	...	...	$\gtrsim 2.50$
152234	−3.9	...	...	$\gtrsim 4.17$
	+3.1	+2.2	+0.9	$2.11^{+1.03}_{-0.61}$
152235	−4.7	−5.0	+0.3	$1.45^{+0.84}_{-0.37}$
	+1.1	+0.2	+0.9	$0.77^{+0.59}_{-0.24}$
152236	−7.7	−9.9,−3.3	?	$0.47^{+0.26}_{-0.22}$
	...	+0.8	...	$\lesssim 0.34$
152248	+3.1	+2.2	+0.9	$1.20^{+0.47}_{-0.53}$
152249	−3.4	...	...	$\gtrsim 5.00$
	+3.1	+2.2	+0.9	$2.44^{+1.55}_{-0.94}$
152270	+3.1	+2.2	+0.9	$1.17^{+0.53}_{-0.38}$
152408	−3.3	...	...	$\gtrsim 0.45$
152424	...	−17.0	...	$\lesssim 1.15$
	−11.4	−11.5	+0.1	$1.05^{+0.87}_{-0.27}$
	−3.9	−4.1	+0.2	$1.67^{+0.93}_{-0.67}$
	...	+1.0	...	$\lesssim 0.42$
	+4.1	...	...	$\gtrsim 4.17$

was detected at a velocity more negative than -20 km s^{-1}. For comparison, the OB association itself has a radial velocity of about -25 ± 5 km s^{-1} (*cf.* the discussion given in § IV (a) of Crawford *et al.* 1989) so none of the observed molecular components are likely to arise in its vicinity. On the other hand, the observed velocity range of the molecular absorption corresponds to that expected for foreground clouds co-rotating with the Galaxy, and has been found (Crawford *et al.* 1989) to be occupied by strong Na I and Ca II absorption lines. It seems clear that the molecular components arise in some of the foreground diffuse clouds which were postulated by Crawford *et al.* (1989) to explain the low-velocity ($-20 \lesssim v_{\rm helio} \lesssim 0$ km s^{-1}) Na I and Ca II absorption. [Note, however, that detailed modelling of the Na I absorption (Crawford 1988, pp. 104–113) has indicated that additional Na I components, not associated with molecular absorption, are also present in this velocity range.] As discussed in Section 1, there is evidence that these clouds occur within about 700 pc of the Sun.

The stars HD 152234, 152248, 152249 and 152270 are all members of the cluster NGC 6231, and have projected separations of $\lesssim 2$ pc at a distance of 1900 pc (and $\lesssim 0.8$ pc for a distance of 700 pc). All four stars exhibit a CH component at $v_{\rm helio} \sim +2.2$ km s^{-1} and a CH^+ component at $v_{\rm helio} \sim +3.1$ km s^{-1}. Following the discussion in Section 5, these are

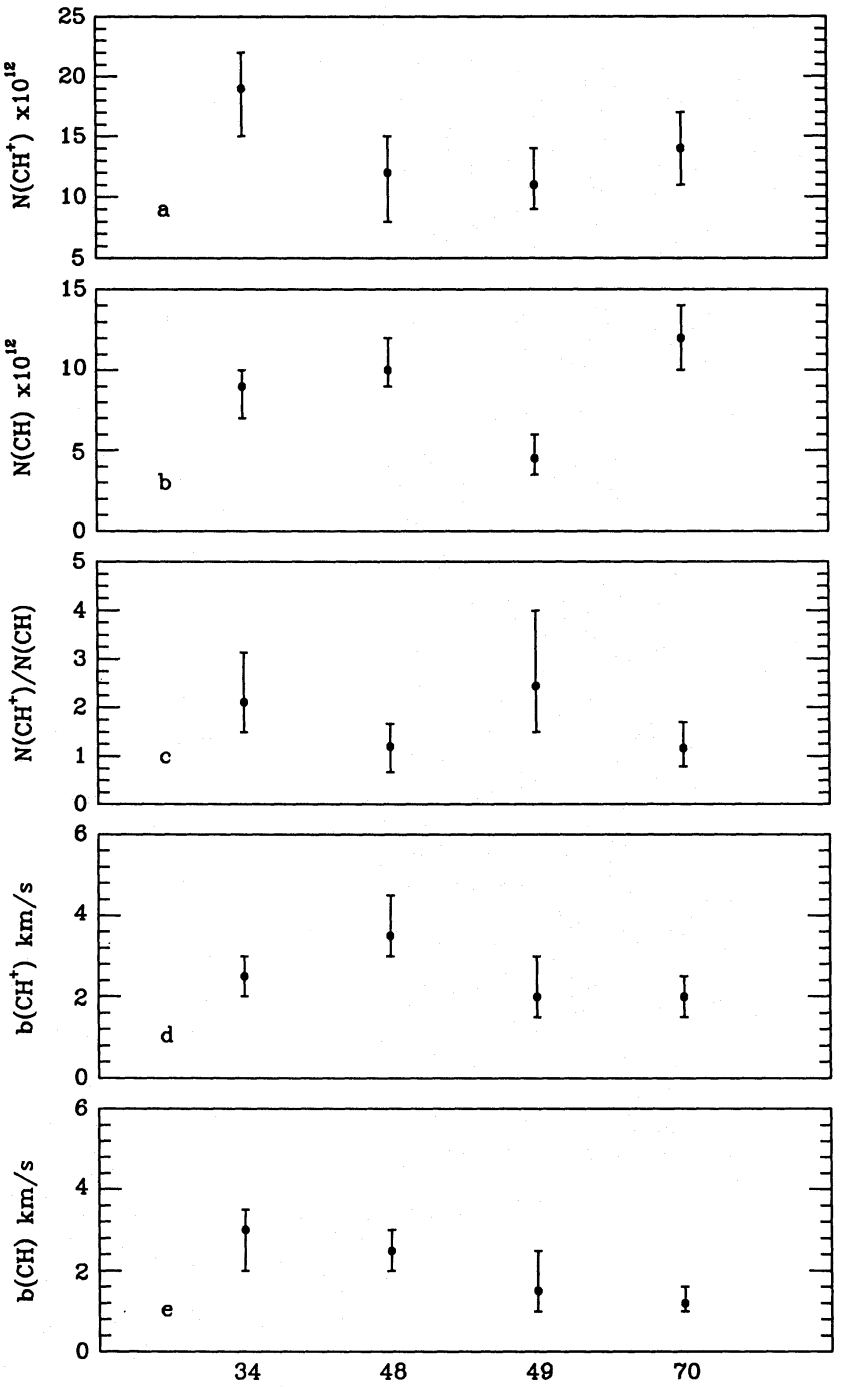

Figure 10. A comparison of molecular column densities and velocity dispersions for the common velocity component observed towards four members of the central cluster NGC 6231. The stars are identified by the last two digits of their HD numbers.

assumed to be due to the same cloud of material. Since these components are common to all four stars, they presumably arise in a single foreground cloud whose angular extent on the sky is comparable to that of the cluster (4 arcmin). This material cannot occupy a significantly larger area of sky because components at these velocities do not occur towards any other of the association stars. The column densities, CH^+/CH ratio, and velocity dispersions for these 'common' components are shown in Fig. 10. It can be seen that these values are similar for all four stars, but that some variations, particularly in the column densities, do exist. Thus,

although this material is located as a body over about 4 arcmin of sky, it is not completely homogeneous.

Although there is only one CH component towards the four stars discussed above, both HD 152234 and 152249 (Figs 2 and 6) have additional CH$^+$ components at -3.9 and -3.4 km s^{-1}, respectively. Due to the errors on the quoted velocities, the 0.5 km s^{-1} difference between them cannot be considered significant, but the fact that a CH$^+$ component at this velocity is not seen towards HD 152248 (Fig. 5), which lies between HD 152234 and 142249 on the sky [*cf.* fig. 1 of Crawford *et al.* (1989)] argues against them being due to the same material. It is interesting that the lower limits to the CH$^+$/CH ratio, derived from the non-detection of a corresponding CH component, are 4.2 and 5.0, respectively. These are significantly larger than the values that were found for the 'common' velocity components towards these stars (Fig. 10c). It appears that in these components some mechanism has greatly enhanced the CH$^+$/CH ratio (*cf.* Section 8).

Outside the tight grouping of NGC 6231 it is difficult to find common velocity components. There are three possible identifications that can be made.

(1) A good case can be made for the $+0.8$ and $+1.0$ km s^{-1} CH components seen towards HD 152236 and 152424, respectively, being due to the same material. Not only do they have essentially identical velocities, they also have an unusually small CH$^+$/CH ratio, with only upper limits being recorded (Table 5). These stars are separated by about 20 arcmin (11 pc at a distance of 1900 pc, although only 4 pc at a distance of 700 pc) and a common component would not necessarily be observed towards any other association member (*cf.* fig. 1 of Crawford *et al.* 1989). It is possible that this CH component is related to the $+0.2$ km s^{-1} CH component observed towards HD 152235, although the velocity difference is slightly larger than would be expected from measuring error alone and the CH$^+$/CH ratios are rather different.

(2) It is possible that the -4.7 km s^{-1} and -3.9 km s^{-1} CH$^+$ (and associated CH) components towards HD 152235 and 152424 are related. The velocity difference is at the limit of that which can be explained by measuring error, but the CH$^+$/CH ratios are very similar. These stars are separated by about 13 arcmin on the sky and, again, a common component would not necessarily show up towards any other star.

(3) One of the CH$^+$ components towards HD 152424 has the same velocity (-3.9 km s^{-1}) as the high CH$^+$/CH ratio component towards HD 152234 discussed above. However, this is probably coincidental, since it is not observed towards other stars that lie between these two on the sky, and because in the case of HD 152424 it can be identified with a CH component which yields a CH$^+$/CH ratio much smaller than the lower limit obtained for HD 152234 (Table 5).

Finally, we note that observations of the R(0) line of CN (Crawford 1988) revealed a component with a heliocentric velocity of $+0.8$ km s^{-1} (and a column density of about 1.7×10^{12} cm^{-2}) towards HD 152236. This is the same velocity as the strongest CH component towards this star, and so the two may be assumed to exist in the same cloud. Note that the agreement between these CN and CH components supports the new CH rest wavelength adopted by Black & van Dishoeck (1988); use of the older Moore & Broida (1959) value would result in a 0.5 km s^{-1} difference between them.

7 The number of absorption components, and their column densities, as a function of interstellar reddening

Given the patchy nature of the interstellar extinction across the association (van Genderen *et al.* 1984), it is interesting to see if the number of observed molecular components correlates in

any way with the reddening. Fig. 11 shows the number of discrete components observed for each star as a function of its $E(B-V)$. Of course, the number of identified components is governed to some extent by the signal-to-noise ratio of the observations; Danks, Federman & Lambert (1984) did observe weak CH components towards HD 151804 and 152408 which were not observed here (Section 4). Nevertheless, the ordinate in Fig. 11 can be taken as the number of components with $N \gtrsim 4 \times 10^{12}$ cm^{-2} for both CH and CH$^+$. Fig. 11 shows that the number of observed CH components does increase with $E(B-V)$, at least approximately, whereas there is no such correlation for CH$^+$. It follows that the CH components are associated with enhancements in the density of interstellar dust, whereas for CH$^+$ the situation is more complicated.

Fig. 12 shows the *total* CH$^+$ and CH column densities plotted against $E(B-V)$. It can be seen that the column densities of *both* species increase linearly with reddening and with

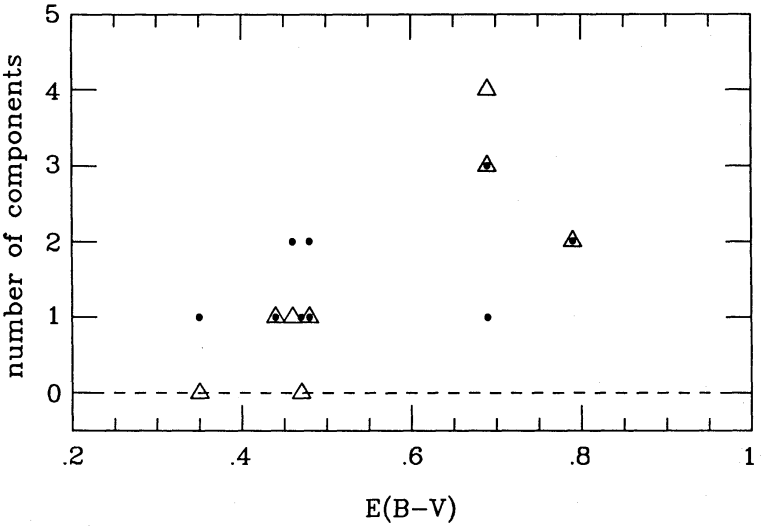

Figure 11. The number of discrete velocity components observed towards the Sco OB1 stars plotted as a function of interstellar reddening. Dots = CH$^+$ components; triangles = CH components.

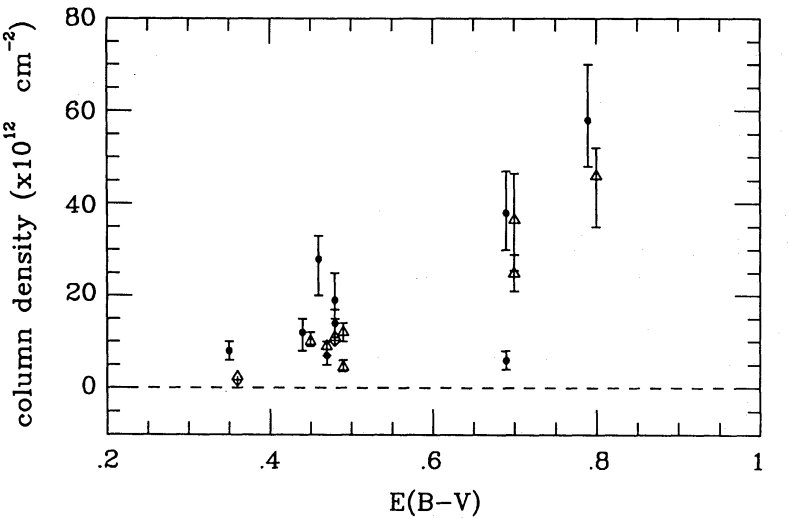

Figure 12. The total CH$^+$ and CH column densities observed towards the Sco OB1 stars plotted as a function of interstellar reddening. Dots = CH$^+$; triangles = CH. In order to avoid points overlapping, those representing CH have been offset to the right by 0.01 mag. The two CH upper limits are indicated by triangles with downward pointing arrows.

essentially the same gradient (weighted least square fits yield gradients of 74 ± 15 and 75 ± 14 cm^{-2} mag^{-1} for CH^+ and CH, respectively, if we exclude the anomalously weak CH^+ column density found for HD 152236). Moreover, both plots exhibit a value of $E(B-V) \sim 0.30$ at zero column density (the least square fits yield 0.27 ± 0.11 and 0.35 ± 0.12 for CH^+ and CH, respectively). Thus it appears that the line-of-sight to Sco OB1 contains a substantial quantity of material (corresponding to a colour excess of about 0.3 magnitudes) that is not associated with molecular material. The *number* of identified CH components (Fig. 11) also falls to zero at about this value of $E(B-V)$, indicating that discrete molecule-bearing clouds are responsible for larger reddenings. The ~ 0.3 mag of colour excess not associated with these molecular clouds is presumably contributed by the clouds responsible for the extra Na I absorption discussed above, the high velocity ($-50 \lesssim v_{helio} \lesssim -20$ km s^{-1}) components which occur towards these stars (discussed by Crawford *et al.* 1989), and any intercloud medium that may be present.

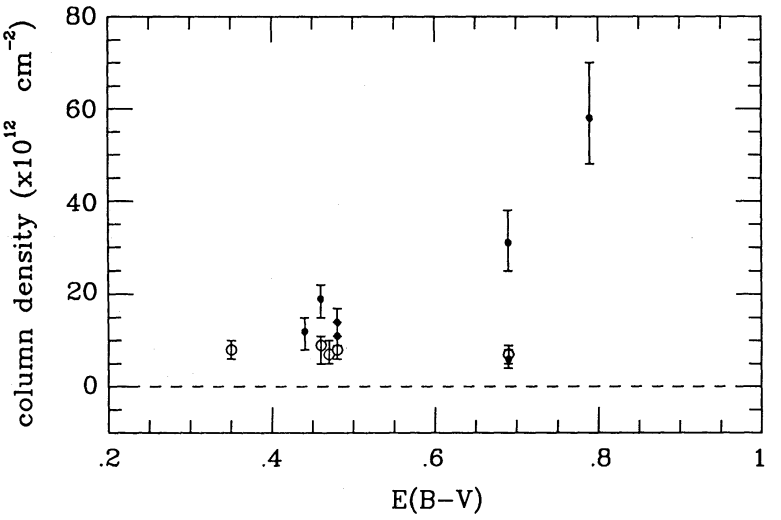

Figure 13. Dots = the CH^+ column densities in components that were judged to correspond to CH components, plotted against the reddening of the star towards which they were observed; open circles = the CH^+ column densities in components which are not associated with CH absorption. See text for discussion.

Fig. 13 (dots) shows the column density in the CH^+ components that were judged to correspond to CH components (Table 5) plotted against the reddening of the star. All of these components have CH^+/CH ratios between about 1.0 and 2.5 (Table 5, excluding HD 152236 for which the ratio is apparently lower, but for which the CH^+ component cannot readily be identified with a CH component). The gradient of the curve is slightly greater than those in Fig. 13 (a weighted least squares fit gives a value of 97 ± 22 cm^{-2} mag^{-1}). This correlation presumably follows directly from the physical association of *these* CH^+ components with CH, the latter of which appears to trace the distribution of interstellar dust towards the OB association. The open circles in Fig. 13 show the column densities in the CH^+ components that are *not* associated with any corresponding CH component as a function of reddening. All of these components have a CH^+/CH ratio $\gtrsim 2.5$, except in the case of HD 152408 for which the ratio could be smaller. We see that for these components there is apparently no dependence of column density on reddening, suggesting that they contribute little dust to the line-of-sight. Clearly, though, it would be necessary to obtain additional observations before being sure of this conclusion.

8 Discussion

Although diffuse cloud chemical models are generally capable of reproducing the CH column densities found in the interstellar medium (e.g. van Dishoeck & Black 1986), these models have proved incapable of producing the observed abundance of CH^+ (see Dalgarno 1976 for a review). For the particular lines of sight considered here, Crawford (1988) found that a simple chemical model, based on the ideas of Federman (1982), was able to account for the observed CH column densities provided that the clouds have densities $n \gtrsim 100$ cm^{-3}. In keeping with many previous results, the CH^+ abundance predicted by this scheme fell short of the observed column densities by more than two orders of magnitude.

The failure of equilibrium chemical models to account for the observations of CH^+ led Elitzur & Watson (1978, 1980) to suggest that CH^+ might be produced in the hot gas immediately behind interstellar shockwaves. They found that moderately strong shocks ($v_s \gtrsim 12$ km s^{-1}) were capable of producing CH^+ column densities of $\sim 10^{13}$ cm^{-2}, although more recent calculations (e.g. Mitchell & Watt 1985; Pineau des Forêts *et al.* 1986) have shown that non-magnetic shocks still produce too little CH^+ by perhaps an order of magnitude. Pineau des Forêts *et al.* (1986) and Draine & Katz (1986) have considered CH^+ production in magnetic shocks. Pineau des Forêts *et al.* found that shocks with $v_s \gtrsim 12$ km s^{-1}, in the presence of a magnetic field of strength ~ 5 μG, were capable of producing CH^+ column densities in excess of 10^{13} cm^{-2}.

In a non-magnetic shock, the hot post-shock gas is accelerated to three-quarters of the shock velocity, and its density increases by a factor of four over the pre-shock value. As it cools, it continues to accelerate, until far from the shock front its velocity is equal to v_s. The density increases as the gas cools, so that far from the shock the density may be several hundred times the pre-shock value (e.g. Spitzer 1978, p. 221). Thus a line-of-sight perpendicular to a shock propagating towards the observer would sample three distinct regions: (1) cold, low-density pre-shock gas, (2) hot, post-shock gas with a density four times the pre-shock value (the presumed site of CH^+ formation), and (3) cold, high-density post-shock gas, blue-shifted by v_s relative to the pre-shock gas, where other molecules (including CH) are thought to form. Note, however, that the presence of a magnetic field will alter this simple picture.

From the results presented here, it appears that there are three distinct types of molecular absorption component towards the Sco OB1 association: components observed in both CH and CH^+, components observed in CH^+ only, and components observed in CH only. We now consider these three component types in the light of shock theories of CH^+ production.

8.1 Components observed in CH and CH^+

A total of nine of these components were found towards seven of the nine stars observed. They are characterized by a $N(CH^+)/N(CH)$ ratio between about 1.0 and 2.5, and a small velocity difference ($\lesssim 0.9$ km s^{-1}) may exist between the two species (but note the caveats added in Section 5). Interpreted in terms of a shock model, a velocity shift of 0.9 km s^{-1} would correspond to a non-magnetic shock travelling towards the observer with a radial velocity of 3.6 km s^{-1}. This velocity is too low for significant CH^+ production. It would be necessary to postulate a large angle ($\sim 70°$) between the direction of shock propagation and the line-of-sight in order for a 0.9 km s^{-1} velocity difference to correspond to a 10 km s^{-1} shock velocity. Even more extreme angles would be required for those components with velocity differences less than 0.9 km s^{-1} (*cf.* Table 5). Note that, although a magnetic field may result in a different velocity shift from that predicted by non-magnetic shock models, the models of Draine & Katz (1986) indicate a *larger* shift than occurs in the non-magnetic case.

Although the very small velocity differences between the two species seem difficult to reconcile with shock models, the observed $N(CH^+)/N(CH)$ ratios for these components are consistent with the magnetic shock models of Pineau des Forêts *et al.* (1986) for $n(H_2)/n(H) < 1$ and $v_s > 11$ km s^{-1}. Note, however, that these authors do not present models with $n(H_2)/n(H)$ values as low as 0.1 which may be appropriate for diffuse clouds (*cf.* Bohlin, Savage & Drake 1978). A post-shock temperature of 3000 K [corresponding to $v_s \sim 10$ km s^{-1}; *cf.* equation (4) of Elitzur & Watson (1980)] would lead to a CH^+ velocity dispersion of $b = 2$ km s^{-1} in the absence of turbulence. This is consistent with the b values listed in Table 4, although these are not significantly larger than those obtained for CH (Table 3) which ought to form in much colder gas.

The observation that the total column densities of both species in these components increase with reddening (Figs 12 and 13) neither supports nor contradicts the shock hypothesis. If most of the clouds were subject to shocks, then more clouds (and hence reddening) would result in more shocks (and hence more CH^+) along the line-of-sight. However, it is also true that a model which tied the CH^+ abundance to the local gas or dust density would also lead to a correlation between CH^+ and reddening.

Thus, while it seems that the presence of shocks may be able to explain the observed CH^+ abundances in these clouds, the question of their actual existence is far from settled. Given that one of the major predictions of the shock models (namely a significant velocity difference between CH and CH^+) cannot be supported by these observations, the possibility of some other (as yet unidentified) route to CH^+ formation in diffuse clouds should not be discounted.

8.2 COMPONENTS OBSERVED IN CH^+ ONLY

Five such components were observed towards five of the nine stars. The CH^+ column densities found for these components were found to be independent of the stellar reddening (Fig. 13) which seems to imply that they contribute little dust to the line-of-sight, although further observations are required to confirm this. In all cases the CH^+/CH ratio was $\gtrsim 2.5$, and in three of the five cases was $\gtrsim 4$ (Table 5). These lower limits, all based on the non-detection of CH, are significantly higher than found for the other components, and it seems likely that they arise in a different type of cloud.

In this respect, it is interesting to note that the non-magnetic shock models of Mitchell & Watt (1985) do predict very large values of the CH^+/CH ratio for the case where a fast shock ($v_s \sim 20$ km s^{-1}) propagates into a low-density cloud with a low fractional abundance of H_2 (for example $CH^+/CH \geq 8$ for $n = 10$ cm^{-3} and $H_2/H \leq 0.01$; *cf.* their table 3). Moreover, the predicted CH^+ column densities in such a case ($\sim 2.8 \times 10^{12}$ cm^{-2}) are within a factor of two of the lower limits to the CH^+ column densities given for these components in Table 4. The MHD models of Pineau des Forêts *et al.* (1986) appear to show the same trend, even though these authors do not consider such small fractional abundances of H_2 (*cf.* their table 5).

Thus it appears plausible that the components observed only in CH^+ may be due to shocked low-density clouds which contain relatively little H_2. Such an interpretation is consistent with these components contributing little to the reddening of the stars towards which they are observed. Note that a CH^+/CH ratio of 8, for example, would predict a corresponding CH column density of $\sim 1 \times 10^{12}$ cm^{-2}, below the detection limit of the present observations. Clearly the hypothesis that these components arise in shocked low-density clouds could be tested by performing observations with a higher signal-to-noise ratio of these lines-of-sight in an attempt to detect a weak CH counterpart to these CH^+ components. If shocks are responsible, a significant velocity difference (perhaps up to 5 km s^{-1}) should be found between the two species.

8.3 COMPONENTS OBSERVED IN CH ONLY

Two stars (HD 152236 and 152424) were found to have CH components that did not correspond to any CH^+ component. The low upper limits to the CH^+/CH ratios (0.34 and 0.42, respectively, Table 5) suggest that these components may represent another class of diffuse cloud, one that is deficient in CH^+. Since diffuse cloud chemical models are capable of producing the observed CH column densities without recourse to shock models, these components can easily be explained by unshocked diffuse molecular clouds in the line-of-sight. Of course, if the shock model is not accepted as the CH^+ formation mechanism in the other types of cloud observed, any theory invoked to replace it must also account for the non-observance of CH^+ in these components.

9 Conclusions

The major conclusions of this work may be summarized as follows.

(1) The observations revealed multiple velocity structure in the interstellar lines of CH and CH^+ towards the Sco OB1 association. This structure was generally different for different stars, implying an inhomogeneous distribution of foreground clouds.

(2) All the molecular absorption occurs at low heliocentric velocities (between about -10 and $+5$ km s^{-1} for all but one star). The radial velocity of the OB association itself is about -25 km s^{-1}, indicating that none of the observed absorption components are associated with it. On the other hand, their velocities are consistent with clouds in the foreground which are co-rotating with the Galaxy; there is other evidence (*cf.* Section 1) that these clouds occur within about 700 pc of the Sun.

(3) The number of CH components towards a given star was found to increase (approximately) with interstellar reddening (Fig. 11), indicating that different numbers of discrete clouds are responsible for the variation in colour excess across the association. The number of CH^+ components towards a particular star showed no such correlation.

(4) Based on the observation that the CH and CH^+ column densities fall to zero at a colour excess of $E(B-V) \sim 0.3$ (Fig. 12), it was argued that this degree of reddening is contributed to the line-of-sight by material other than the molecular clouds.

(5) Although shocks are generally invoked to explain the occurrence of interstellar CH^+, the present observations found evidence for only a very small velocity difference between the CH and CH^+ components that were identified as arising in the same cloud [$v(CH^+) - v(CH) \lesssim 0.9$ km s^{-1}; *cf.* Table 5]. Interpreted in terms of a non-magnetic shock travelling towards the observer, this would imply a shock velocity of $\lesssim 3.6$ km s^{-1}; published shock models indicate that this is too low for significant CH^+ production. A large angle ($\gtrsim 70°$) between the direction of shock propagation and the line-of-sight, for *all* observed cloud components, would be necessary in order for these observations to be consistent with shock speeds as high as 10 km s^{-1}. This observation may support some other, as yet unidentified, route to CH^+ formation in diffuse interstellar clouds.

(6) In addition to velocity components identified in both species, components were observed in CH and CH^+ alone. Since simple chemical schemes can produce sufficient CH, the former appear to present no difficulty. As for the latter, it is noteworthy that models of fast (~ 20 km s^{-1}) shocks in low-density clouds containing relatively little H_2 (Mitchell & Watt 1985) result in large CH^+/CH ratios. These model ratios are consistent with the lower limits found here, suggesting a possible origin for these components.

Acknowledgments

I thank the Director of the Mt Stromlo and Siding Spring Observatories for the generous amount of telescope time made available for this project, and all those at Mt Stromlo who

acted as my night assistants. It is a pleasure to thank Dr Derek McNally for his continuous support and encouragement throughout this work, and Dr W. B. Somerville for comments on an earlier draft of the manuscript. I thank SERC for financial support and PATT for the allocation of travel money. Bibliographic information was obtained from the SIMBAD data retrieval system of the Astronomical Data Centre, Strasbourg.

References

Baird, K. M. & Bredohl, H., 1971. *Astrophys. J.*, **169,** L83.
Bernath, P. F., 1987. *J. Chem. Phys.*, **86,** 4838.
Black, J. H. & van Dishoeck, E. F., 1988. *Astrophys. J.*, **331,** 986.
Bohlin, R. C., Savage, B. D. & Drake, J. F., 1978. *Astrophys. J.*, **224,** 132.
Bok, B. J., Bok, P. F. & Graham, J. A., 1966. *Mon. Not. R. astr. Soc.*, **131,** 247.
Brazier, C. R. & Brown, J. M., 1984. *Can. J. Phys.*, **62,** 1563.
Carrington, A. & Ramsey, D. A., 1982. *Phys. Scripta,* **25,** 272.
Cowie, L. L. & Songaila, A., 1986. *Ann. Rev. Astr. Astrophys.*, **24,** 499.
Crawford, I. A., 1988. *PhD thesis,* University of London.
Crawford, I. A., 1989. *Comm. Univ. London Obs.,* No. 79.
Crawford, I. A., Barlow, M. J. & Blades, J. C., 1989. *Astrophys. J.*, **336,** 212.
Crawford, I. A., Rees, P. C. T. & Diego, F., 1987. *Observatory,* **107,** 147.
Dalgarno, A., 1976. In: *Atomic Processes and Applications,* p. 110, eds Burke, P. G. & Moiseiwitsch, B. L., North-Holland, Amsterdam.
Danks, A. C., Federman, S. R. & Lambert, D. L., 1984. *Astr. Astrophys.*, **130,** 62.
Davenhall, C., 1977. *UCL, Internal Report.*
Draine, B. T. & Katz, N. S., 1986. *Astrophys. J.*, **310,** 392.
Elitzur, M. & Watson, W. D., 1978. *Astrophys. J.*, **222,** L141.
Elitzur, M. & Watson, W. D., 1980. *Astrophys. J.*, **236,** 172.
Federman, S. R., 1982. *Astrophys. J.*, **257,** 125.
Fuller, N. M. J., 1988. *Starlink User Note No. 86.6.*
Giacchetti, A., Stanley, R. W. & Zalubas, R., 1970. *J. Opt. Soc. Am.*, **60,** 474.
Hoffleit, D. & Jaschek, C., 1982. *The Bright Star Catalogue,* 4th edn, Yale University Observatory.
Humphreys, R. M., 1978. *Astrophys. J. Suppl.*, **38,** 309.
Lambert, D. L. & Danks, A. C., 1986. *Astrophys. J.*, **303,** 401.
Lynds, B. T., 1980. *Astr. J.*, **85,** 1046.
Mitchell, G. F. & Watt, G. D., 1985. *Astr. Astrophys.*, **151,** 121.
Moore, C. E. & Broida, H. P., 1959. *J. Res. Nat. Bur. Stand.*, **63A,** 19.
Norlén, G., 1973. *Phys. Scripta,* **8,** 249.
Pineau des Forêts, G., Flower, D. R., Hartquist, T. W. & Dalgarno, A., 1986. *Mon. Not. R. astr. Soc.*, **220,** 801.
Savage, B. D., Bohlin, R. C., Drake, J. F. & Budich, W., 1977. *Astrophys. J.*, **216,** 291.
Schild, R. E., Neugebauer, G. & Westphal, J. A., 1971. *Astr. J.*, **76,** 237.
Spitzer, L., 1978. *Physical Processes in the Interstellar Medium,* John Wiley, New York.
Stapinski, T. E., Rodgers, A. W. & Ellis, M. J., 1981. *Publs astr. Soc. Pacif.*, **93,** 242.
Strömgren, B., 1948. *Astrophys. J.*, **108,** 242.
van Dishoeck, E. F. & Black, J. H., 1986. *Astrophys. J. Suppl.*, **62,** 109.
van Genderen, A. M., Bijeveld, W. & van Groningen, E., 1984. *Astr. Astrophys. Suppl.*, **58,** 537.
Vogel, S. N., Kulkarni, S. R. & Scoville, N. Z., 1988. *Nature,* **334,** 402.

Note added in proof

While this paper was in press the opportunity occurred to re-observe some of these stars in order to provide a guide to the reliability of the results presented here. The additional results are as follows.

(i) New observations of HD 152270 yielded $v_{\rm helio} = 2.2$ and 2.5 km s^{-1} for CH and CH$^+$, respectively, both $\pm \sim 0.5$ km s^{-1}; the former is identical to the value given in Table 3, while